

## Supplementary Information for

# Ag-nanoparticle-decorated Au-fractal patterns on bowl-like-dimple arrays on Al foil as an effective SERS substrate for the rapid detection of PCBs

Chao Hou,<sup>ab</sup> Guowen Meng, <sup>\*ba</sup> Qing Huang,<sup>c</sup> Chuhong Zhu,<sup>b</sup> Zhulin Huang,<sup>b</sup> Bin Chen<sup>b</sup> and Kexi Sun<sup>b</sup>

<sup>a</sup> University of Science and Technology of China, Hefei, China.

<sup>b</sup> Key Laboratory of Materials Physics, and Anhui Key Laboratory of Nanomaterials and Nanostructures, Institute of Solid State Physics, Chinese Academy of Sciences, Hefei, 230031, China.

*E-mail:* gwmeng@issp.ac.cn

<sup>c</sup> Key Laboratory of Ion Beam Bioengineering, Hefei Institutes of Physical Science, Chinese Academy of Sciences, Hefei, 230031, China.

**The Supplementary Information includes:**

**Part S1: Experimental section**

**Part S2: Energy dispersive X-ray spectroscopy spectra**

**Part S3: The absorption spectra in visible light range**

**Part S4: The Au-fractals achieved with different Au-sputtering durations**

**Part S5: Different structures achieved on different underlying substrates**

**Part S6: The formation mechanism of the Au fractals**

**Part S7: SERS spectra showing good signal reproducibility of the substrate**

**Part S8: Tables**

**Part S9: References**

## Part S1: Experimental section

Firstly hexagonally patterned bowl-shaped-dimple arrays on Al foil were achieved by anodizing high purity (99.999 %) Al foil under 40 V<sub>DC</sub> in a 0.3 M oxalic acid solution at 8 °C for 6 h, followed by completely etching the topmost porous anodic alumina membrane in a mixing solution of 6 wt% phosphoric acid and 1.8 wt% chromic acid at 60 °C for 9 h. Then Au-nanoparticles were sputtered uniformly onto the ordered dimple arrays by using K550X Sputter Coater sputtering apparatus. For the formation of Au-aggregates-assembled fractal patterns, Al foil supported Au-nanoparticles were annealed in Ar at 550 °C for 6 h. For further improving the SERS activity of the Au-fractal patterns, much smaller Ag-nanoparticles were sputtered onto the Au-fractal patterns with a 15 mA current for several minutes. The products were characterized by using field-emission scanning electron microscopy (FE-SEM, Sirion 200, Veeco, 10 kV) and energy dispersive X-ray spectroscopy (EDS, Oxford).

For SERS measurements, the Ag-nanoparticles-decorated Au-aggregates-assembled fractal patterns on ordered bowl-shaped-dimples on Al foil were immersed in 0.5 mL of R6G aqueous solution for 10 h, then taken out and dried in the air. For examining their SERS sensitivity to PCB-77, PCB-77 was firstly dissolved in acetone, then 20 µL of the solution was dispersed on the substrates to enrich PCB-77 molecules on the surfaces of the Ag-nanoparticles-decorated Au-aggregates-assembled fractal patterns, followed by drying in the air to evaporate any moisture. For further improving the detection sensitivity to PCB-77, the Ag-nanoparticles-decorated Au-aggregates-assembled fractal patterns were modified with HS-β-CD by immersing the substrates into HS-β-CD for overnight, then taken out, dried and dispersed with PCB-77 acetone solution and dried. SERS spectra were measured by using a confocal Raman spectrometer (Renishaw Invia, 532 nm laser line, 20×), where the effective power of the laser source was 0.15 mW for R6G, and 0.3 mW for PCB-77, respectively. The laser spot focused on the sample surface was about 10 µm in diameter. During SERS measurement, the acquisition time was 10 s for R6G and 20 s for PCBs, respectively.

## Part S2: Energy dispersive X-ray spectroscopy spectra

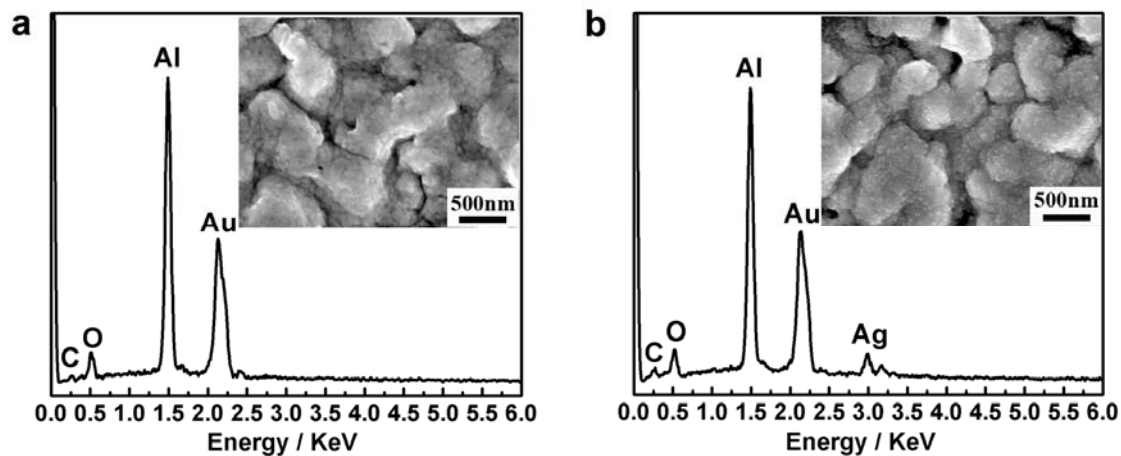


**Fig. S1** Energy dispersive X-ray spectroscopy (EDS) spectra of the Au-fractal patterns before (a) and after (b) decorated with Ag-nanoparticles for 4 min. The insets are corresponding SEM images.

## Part S3: The absorption spectra in visible light range

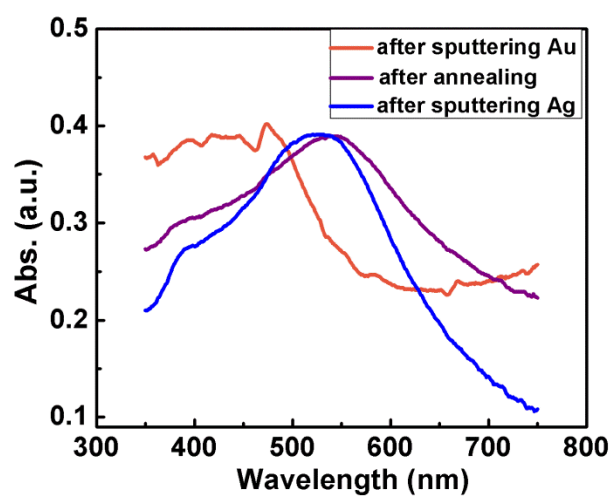


**Fig. S2** The absorption spectra in visible light range of the ordered bowl-like-dimple arrays after sputtering Au-nanoparticles, after annealing, and after decorated with Ag-nanoparticles.

## Part S4: The Au-fractals achieved with different Au-sputtering durations

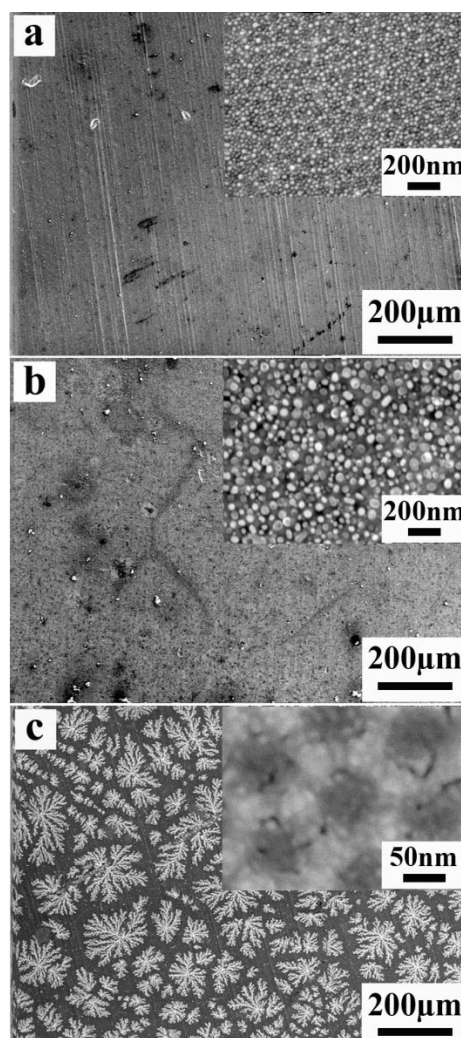


**Fig. S3** SEM images of the Au-fractals achieved by performing the same *in situ* annealing (Ar, 550 °C, 6h) on the Au-nanoparticles with different Au-sputtering durations of 2 min (a), 3 min (b), 4 min (c). Insets in (a) and (b) are corresponding close-up views. Inset in (c) is the SEM image of the ordered bowl-shaped-dimple arrays sputtered with Au-nanoparticles for 4 min before annealing.

## Part S5: Different structures achieved on different underlying substrates

In order to show the importance of underlying substrates on the formation of the Au-aggregates-assembled fractal patterns, we did comparative experiments on the substrates with different surface morphologies such as planar Si wafer (Fig. S4a), wrought Al foil (Fig. S4c), oxalic-acid-treated Al foil (Fig. S4e), and hexagonally patterned bowl-like-dimple arrays on Al foil (Fig. S4g). For the Si wafer, after Au-sputtering and *in situ* annealing, Au branched-structures are formed randomly (Fig. S4b), indicating that Au-nanoparticles on the Si wafer tend to form fractal patterns via self-assembling during annealing. However as the Si wafer surface is very smooth, the Au-nanoparticles prefer to form large-scale particle-assembled film. For the wrought Al foil, a lot of fractals are formed along the scratches on the Al foil (Fig. S4d), indicating that uneven surface defects favor the formation of fractal patterns. In the case of oxalic-acid-treated Al foil, the fractals (Fig. S4f) are denser than those achieved on the wrought Al foil. This can be attributed to the numerous large dimples of various sizes on the oxalic-acid-etched Al foil (Fig. S4e). These dimples with low energy offer preferential locations for the Au-nanoparticles to coalesce and grow up. Thus dimples are critical for the Au-nanoparticles to walk randomly to form fractal architectures. The large-area ordered bowl-shaped-dimples with identical size (Fig. S4g) on Al foil provide a relatively uniform environment for the fusion of the Au-nanoparticles, therefore, the fractals can easily grow up to well-distributed structures (Fig. S4h).

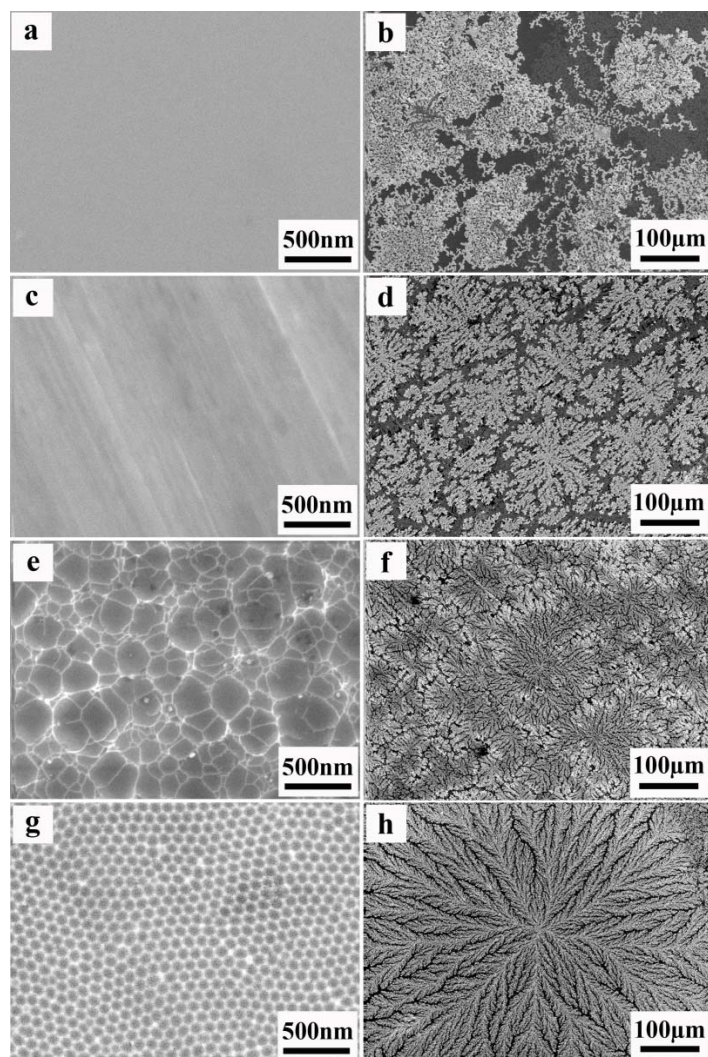


**Fig. S4** The surface morphology of Si wafer (a), wrought Al foil (c), Al foil immersing in 0.3 M oxalic acid for 24 h (e), and the ordered bowl-shaped-dimple arrays (g). (b, d, f, h) are corresponding morphology achieved using the same Au-sputtering duration (16 min) and annealing for 6 h.

## Part S6: The formation mechanism of the Au fractals

As for the fractals formation mechanism, there are two models of diffusion-limited aggregation<sup>1</sup> and random-successive nucleation<sup>2</sup>, which are usually accepted. In the diffusion-limited aggregation model of a simple square lattice, randomly diffusing particles are added one by one from the sites far from a central cluster, and stick irreversibly at the first contact with the growing aggregate. The formation of our Au fractal patterns can be ascribed to the combination of Ostwald ripening and diffusion-limited aggregation of Au-nanoparticles. Ostwald ripening<sup>3</sup> is a spontaneous process in which small particles grow into large ones as the large particles are more energetically favored than the small ones. During the *in situ* annealing, the sputtered small Au-nanoparticles on the ordered dimple arrays firstly fuse together to fill up every dimple (Fig. S5c) as large particles with greater volume to surface area ratios have a lower energy state, and the energy state near the each dimple center is the lowest so the aggregating particle will preferentially settle down on the dimple center. With the increase of annealing temperature, the Au-particles grow larger and larger to further decrease their interfacial free energy. This growing-up process of Au-nanoparticles (Fig. S5d–f) induced by Ostwald ripening will continue until a relatively large particle (Fig. S5f) randomly appear on the substrate as the center (or nuclear site) of a fractal shape. A second particle walk randomly until it visits a site adjacent to the above-mentioned center as part of the aggregate. Another particle elsewhere walks randomly until it joins the aggregate, and so forth. The experimentally observed growing fractal shapes from Fig. S5f to Fig. S5h are in accordance with the diffusion-limited aggregation theory. This process continues until pieces of snowflake-like fractal patterns (Fig. S5i) are formed.

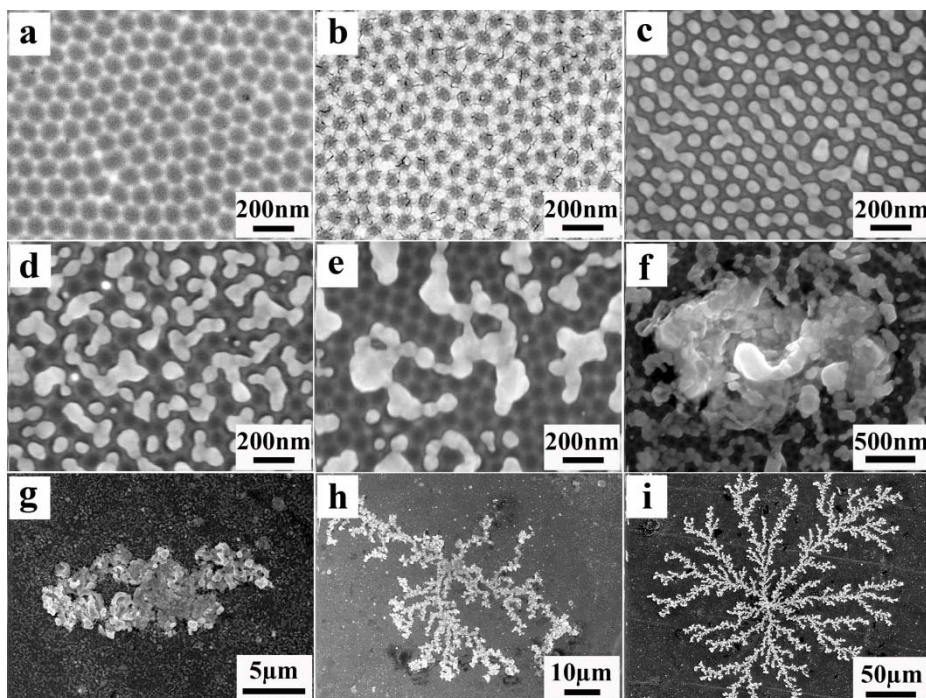


**Fig. S5** (a) Empty ordered bowl-shaped-dimple arrays. (b) Sputtering with Au-nanoparticles for 4 min. The morphologies achieved by heating the sputtered ordered bowl-shaped-dimple arrays to 400 °C (c), 450 °C (d), 500 °C (e) in Ar atmosphere and then cool down in furnace. (f–h) Three different places observed after heating to 550 °C followed by furnace cooling (the three different observation areas of the same sample are demonstrated to show this process). (i) Annealing at 550 °C for 3 h.

## Part S7: SERS spectra showing good signal reproducibility of the substrate

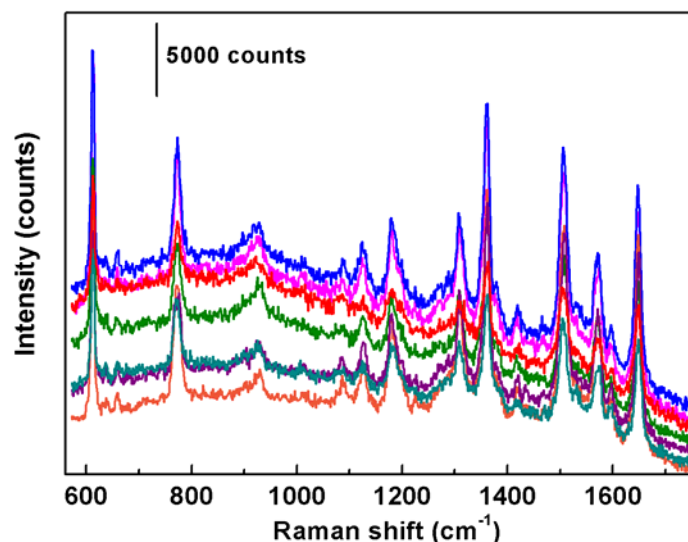


**Fig. S6** SERS spectra of  $10^{-7}$  M R6G aqueous solution on seven chosen spots of the Ag-nanoparticles-decorated Au-aggregates-assembled fractal patterns with 4 min-Ag-sputtering time, demonstrating good signal reproducibility of the substrate. The acquisition time was 10 s for each spot with a 532 nm laser line.

## Part S8: Tables

**Table S1.** The statistical results of average sizes and numbers of fractals per square millimeter by tailoring Au-nanoparticles sputtering durations.

Statistical results	4 min	8 min	12 min	16 min
one piece of fractal ( $\mu\text{m}$ )	88	163	336	432
self-assembled Au-aggregates (nm)	449	463	498	516
numbers of fractals per $\text{mm}^2$	64.4	18.2	5.4	3.2

**Table S2.** The statistical results of average sizes and numbers of fractals per square millimeter by tailoring annealing durations.

Statistical results	10 min	1 h	3 h	6 h
one piece of fractal ( $\mu\text{m}$ )	190	221	280	432
self-assembled Au-aggregates (nm)	466	473	508	516
numbers of fractals per $\text{mm}^2$	26.0	18.2	9.8	3.2

## Part S9: References

- 1 H. Röder, K. Bromann, H. Brune, K. Kern, *Phys. Rev. Lett.* 1995, **74**, 16.
- 2 (a) Z. W. Chen, S. Y. Zhang, S. Tan, M. L. Tian, J. G. Hou, Y. H. Zhang, *Thin Solid Films*. 1998, **322**, 194; (b) J. G. Hou, Z. Q. Wu, *Phys. Rev. B*. 1990, **42**, 3271.
- 3 P. W. Voorhees, *J. Stat. Phys.* 1985, **38**, 1.